Improving oxidation resistance of Ni-16Mo-7Cr-4Fe nickel-based superalloy by yttrium microalloying: Postprint

Authors: LI Xiao-Li, HE Shang-Ming, ZHOU Xing-Tai, LI Zhi-Jun, ZOU Yang, LI Ai-Guo, YU Xiao-Han

Date: 2023-06-18T00:00:00+00:00

Abstract

Microstructure and oxidation behavior of modified Ni-16Mo-7Cr-4Fe alloys by yttrium microalloying were investigated by scanning electron microscopy, transmission electron microscopy, grazing incident X-ray diffraction and synchrotron radiation X-ray fluorescence. M6C and Ni17Y2 phases were observed and the amount of Ni17Y2 increased with yttrium concentration. When the yttrium concentration increased to 0.43wt.%, some Ni17Y2 chains and multi phase regions containing Ni17Y2, M6C and γ phase appeared, which is harmful for the oxidation resistance. The alloy containing 0.05wt.% yttrium showed the best oxidation resistance, which derives its oxidation resistance from the adequate concentration of yttrium in the solid-solution (γ phase), the formation of the protective layer of YCrO3 and chromia oxide and the strengthening effect of yttrium on oxide boundaries.

Full Text

Preamble

Improving Oxidation Resistance of Ni-16Mo-7Cr-4Fe Nickel-Based Superalloy by Yttrium Microalloying

LI Xiao-Li,[1] HE Shang-Ming,[2],† ZHOU Xing-Tai,[1] LI Zhi-Jun,[1] ZOU Yang,[1] LI Ai-Guo,[2] and YU Xiao-Han[1],‡

[1]Shanghai Institute of Applied Physics, Chinese Academy of Sciences, 2019 Jialuo Road, Shanghai 201800, China
[2]Shanghai Synchrotron Radiation Facility (SSRF), Shanghai Institute of Applied Physics, Chinese Academy of Sciences, 239 Zhangheng Road, Shanghai 201204, China

(Received July 8, 2014; accepted in revised form September 9, 2014; published online June 20, 2015)

Abstract: The microstructure and oxidation behavior of yttrium-microalloyed Ni-16Mo-7Cr-4Fe alloys were investigated using scanning electron microscopy, transmission electron microscopy, grazing-incidence X-ray diffraction, and synchrotron radiation X-ray fluorescence. M_6C and $Ni_{17}Y_2$ phases were observed, with the amount of $Ni_{17}Y_2$ increasing with yttrium concentration. When the yttrium concentration reached 0.43 wt.%, $Ni_{17}Y_2$ chains and multi-phase regions containing $Ni_{17}Y_2$, M_6C, and γ phase appeared, which proved detrimental to oxidation resistance. The alloy containing 0.05 wt.% yttrium exhibited the best oxidation resistance, deriving its protective properties from an optimal yttrium concentration in the solid-solution (γ phase), the formation of a protective $YCrO_3$ and chromia oxide layer, and the strengthening effect of yttrium on oxide grain boundaries.

Keywords: Nickel-based superalloy, Molten salt reactor, Rare earth yttrium, Microstructure, Oxidation, X-ray fluorescence

DOI: 10.13538/j.1001-8042/nst.26.030201

Introduction

Developing relatively clean nuclear energy represents an effective solution to the energy crisis, and structural materials for nuclear reactors are crucial to operational safety. The Ni-16Mo-7Cr-4Fe alloy, manufactured by the Institute of Metal Research, Chinese Academy of Sciences, is a nickel-based superalloy similar to Hastelloy N, which was developed in the 1960s at Oak Ridge National Laboratory for constructing molten fluoride salt containers. This alloy is known for its excellent resistance to corrosion, oxidation, neutron irradiation, and high-temperature degradation in molten salt reactors (MSRs) [1].

In China' s efforts to develop the next-generation MSR, Ni-16Mo-7Cr-4Fe alloy will serve as a structural material that must withstand the harsh environment of molten fluoride salts at high temperatures (1073 K or higher). This alloy requires protection from external oxidation at elevated temperatures, as air oxidation can lead to coolant tube leaks during service [2, 3]. The high-temperature oxidation resistance of Ni-16Mo-7Cr-4Fe alloy does not meet the requirements of next-generation MSRs, a problem that may be solved through rare earth microalloying modifications.

Yttrium, as a rare earth element, has been successfully applied in metallurgy [4–11] and chemical and surface engineering [12–17]. Recently, yttrium has emerged as a promising alloying element for superalloys, improving the oxidation resistance of nickel-based alloys [7], Fe-Ni-Cr ternary alloys [18], and Co-based alloys [19]. Beneficial effects of yttrium doping include promoting the formation of compact oxide layers, facilitating phase transformations, mitigating harmful phases by counteracting deleterious elements [7, 18, 20–22], and forming fine

dendrites [23]. However, to the authors' knowledge, little research has focused on the effects of yttrium in the matrix on the oxidation resistance of Ni-based superalloys. In this study, synchrotron radiation X-ray fluorescence (SRXRF) was employed to determine the distribution and content of trace yttrium in the matrix, which influences the microstructure and oxidation resistance of Ni-16Mo-7Cr-4Fe alloy. This work helps extend the usable critical temperature of nickel-based superalloys for molten salt energy systems.

II. Materials and Methods

Master alloys supplied by the Institute of Metal Research, Chinese Academy of Sciences (Shenyang, China) were melted in a vacuum induction furnace, with varying amounts of yttrium added to obtain Ni-16Mo-7Cr-4Fe alloys (designated G00, G05, G12, G21, and G43). The chemical compositions determined by ICP-AES (inductively coupled plasma atomic emission spectroscopy) are presented in Table 1 . The ingots were hot-rolled at 1453 K to sheets approximately 2 mm thick, then homogenized at 1450 K for 10 minutes and aged at 1173 K for 20 hours in a KSL-1400X muffle furnace, followed by water quenching.

Test specimens ($22 \times 8 \times 2$ mm^3) were cut from the sheets and subsequently ground, polished, and cleaned. Oxidation testing was conducted at 1273 K in air using a KSL-1400X muffle furnace. Weight changes were measured using an ESJ180-4 electric balance with 0.1 mg accuracy after each exposure period, with five specimens tested to obtain average values. Microstructure before and after oxidation testing was examined using a LEO 1530VP scanning electron microscope (SEM) and a Tecnai G2 F20 transmission electron microscope (TEM) equipped with energy dispersive spectroscopy (EDS). X-ray fluorescence (XRF) at 20.5 keV and grazing-incidence X-ray diffraction (GIXRD) at 10.0 keV were performed at the Shanghai Synchrotron Radiation Facility (SSRF).

III. Results and Discussion

Figure 1 shows SEM images of the Ni-16Mo-7Cr-4Fe alloys before oxidation. Coarse particles were observed along grain boundaries, with their number increasing with yttrium concentration. SEM-EDS analysis identified these as Mo-rich and Y-rich phases. The quantity of Y-rich phase increased with yttrium concentration, while the Mo-rich phase content in G05 was lower than in G00 but increased with further yttrium addition. TEM analysis confirmed these phases as M_6C and $Ni_{17}Y_2$, respectively.

The selected area diffraction patterns (SADPs) of M_6C and $Ni_{17}Y_2$ are shown in Fig. 2 [FIGURE:2]. M_6C exhibits an angular morphology with a face-centered cubic structure, while $Ni_{17}Y_2$ has a hexagonal crystal structure (a = 0.8320 nm, c = 0.8042 nm, space group $P6_3/mmc$). Figure 3 [FIGURE:3] presents TEM micrographs of these phases. The $Ni_{17}Y_2$ morphology transitioned from round to irregular as yttrium content increased, appearing circular in G05 (Fig. 3(a)) and growing into irregular shapes (Fig. 3(b)). At 0.43 wt.% yttrium,

multi-phase regions containing M_6C and $Ni_{17}Y_2$ emerged (Fig. 3(c)). The M_6C phase appeared as strips in G00 (Fig. 3(d)), changed to discrete particles in G05 (Fig. 3(e)), and reverted to strip morphology at higher yttrium concentrations (Fig. 3(f)).

Oxidation curves for all specimens are shown in Fig. 4(a). Yttrium addition substantially improved the oxidation resistance of Ni-16Mo-7Cr-4Fe alloy, with G05 showing the best performance. However, oxidation resistance gradually deteriorated as yttrium concentration increased further. Proper yttrium content significantly enhanced oxide scale adhesion to the substrate, as evidenced by the mass of spalled scale shown in Fig. 4(b). Severe spallation did not occur in G05 after 300 hours, whereas G00 exhibited the most severe spalling, followed by G43, G21, and G12.

GIXRD analysis of oxide scales on G00 and G05 (Fig. 5 [FIGURE:5]) revealed that both outermost layers consisted of NiO (PDF 65-6920) and $NiFe_2O_4$ (PDF 47-1417). Cross-sectional XRF mapping (Fig. 6 [FIGURE:6]) showed that most of the outer oxide layer in G00 and G43 had spalled. The small mapping area (100 µm × 300 µm) prevented clear detection of the outmost Ni/Fe-rich layer (Fig. 6(b)). The oxide scale on G05 was significantly thinner and more compact than those on G00 and G43 (Fig. 6). For G00, only NiO and $NiFe_2O_4$ were detected until the incidence angle reached approximately 10°, at which point Cr_2O_3 (PDF 38-1479), minor spinel oxides ($NiCrMnO_4$, PDF 020-0780; $NiCr_2O_4$, PDF 23-1272; $FeCr_2O_4$, PDF 24-0511), and the matrix appeared. NiO and $NiFe_2O_4$ diffraction peaks persisted at this higher angle. At 15°, matrix and spinel oxide diffraction intensities increased markedly. In contrast, for G05, diffraction peaks corresponded mainly to NiO and $NiFe_2O_4$ at 0.1° incidence. At 0.5°, Cr_2O_3, $YCrO_3$, spinel oxides ($NiCrMnO_4$, $NiCr_2O_4$, $FeCr_2O_4$), and the matrix emerged. At 0.8°, matrix and spinel oxide diffraction intensities increased significantly. These results indicate that the oxide scale on G00 is much thicker than that on G05.

Several factors may explain these observations. First, G05 exhibited higher yttrium concentration in the matrix than G43, as revealed by Y mapping in Fig. 6 and EPMA analysis in Fig. 7 [FIGURE:7]. As yttrium content increases, the volume fraction of $Ni_{17}Y_2$ increases (Fig. 7(a)) while the yttrium concentration in the matrix decreases (Fig. 7(b)). Consequently, internal compact layers of $YCrO_3$, Cr_2O_3, and spinel oxides form more readily in G05, hindering Mo diffusion. Second, interfaces between coarse $Ni_{17}Y_2$ particles and the matrix in alloys with excess yttrium may provide diffusion channels for oxygen and oxidizable elements, particularly Mo. Therefore, no Mo-rich layer was observed in the oxide scale of G05, which contained the smallest amount of $Ni_{17}Y_2$, whereas Mo-rich layers in G00 and G43 were quite thick. Third, proper yttrium addition can strengthen oxide grain boundaries at the surface. Figure 8 [FIGURE:8] shows the surface oxide morphology after 100 hours at 1273 K. No cracks appeared on G05, while intergranular cracks were evident on G00. It is suggested that proper yttrium addition may form internal oxide boundaries where vacancies

can condense, thereby reducing void formation [24] and enhancing oxide grain boundary strength.

IV. Conclusion

Proper yttrium addition improves the distribution of coarse M_6C particles. The number and size of detrimental $Ni_{17}Y_2$ phases increase with yttrium concentration, and their morphology changes from round to irregular. At 0.43 wt.% yttrium, coarse $Ni_{17}Y_2$ chains and multi-phase regions containing $Ni_{17}Y_2$, M_6C, and γ phase appear.

Yttrium microalloying improves the oxidation resistance of Ni-16Mo-7Cr-4Fe alloy at 1273 K. The alloy containing 0.05 wt% yttrium forms the thinnest and most compact oxide scale. Proper yttrium promotes formation of a compact internal $YCrO_3$ and Cr-O oxide layer, thereby inhibiting Mo diffusion. However, as yttrium concentration increases further, oxidation resistance decreases because coarse $Ni_{17}Y_2$ consumes most of the yttrium in the matrix, reducing its beneficial strengthening effect.

Acknowledgements

The authors thank the staff at the BL15U and BL14B beamline stations of SSRF.

References

[1] Huntley W R and Gnadt P A. Design and operation of a forced-circulation corrosion test facility (MSR-FCL-1) employing hastelloy N alloy and sodium fluoroborate salt. Oak Ridge National Laboratory Report, ORNL-TM-3863, 1973.
[2] McNeese L E. Molten salt reactor program. Oak Ridge National Laboratory Report, ORNL-5047, 1975, 125–150.
[3] McNeese L E. Molten salt reactor program. Oak Ridge National Laboratory Report, ORNL-5132, 1976, 1–15.
[4] Bullock E, Lea C, McLean M. Benefits of minor additions of yttrium to the oxidation and creep behavior of a nickel-based composite. Philos T R Soc A, 1980, 295: 332–333. DOI: 10.1098/rsta.1980.0126
[5] Hsu C G and Pan J M. Reaction of yttrium with p-nitrochlorophosphonazo and the spectrophotometric determination of yttrium in nickel-base alloys in the presence of cerium sub-group rare earths. Analyst, 1985, 110: 1245–1248. DOI: 10.1039/an9851001245
[6] Sato A, Sato A, Harada H, et al. Creep strength of yttrium doped 4th generation Ni-base single crystal superalloy. J Japan Inst Metals, 2006, 70: 380–383. DOI: 10.2320/jinstmet.70.380
[7] Stott F H, Wood G C, Fountain J G. The influence of yttrium additions on the oxidation resistance of a directionally solidified Ni-Al-Cr3C2 eutectic alloy. Oxid Met, 1980, 14: 135–146. DOI: 10.1007/bf00603990

[8] Vozzella P A and Condit D A. Determination of yttrium in complex nickel-base alloys using microwave dissolution and inductively coupled plasma optical emission spectrometry. Anal Chem, 1988, 60: 2497–2500. DOI: 10.1021/ac00173a013
[9] Xiao C B and Han Y F. Effect of yttrium on diffusion layer of Ni-Al-Mo-B alloy IC6 during high temperature oxidation process. Scripta Mater, 1999, 41: 1217–1221. DOI: 10.1016/s1359-6462(99)00277-8
[10] Zhou P J, Yu J J, Sun X F, et al. Influence of Y on stress rupture property of a Ni-based superalloy. Mat Sci Eng A-Struct, 2012, 551: 236–240. DOI: 10.1016/j.msea.2012.04.117
[11] Zhou P J, Yu J J, Sun X F, et al. Role of yttrium in the microstructure and mechanical properties of a boron-modified nickel-based superalloy. Scripta Mater, 2007, 57: 643–646. DOI: 10.1016/j.scriptamat.2007.06.003
[12] Wang S X, Li C, Xiong B J, et al. Surface modification of hard alloy by Y ion implantation under different atmosphere. Appl Surf Sci, 2011, 257: 5826–5830. DOI: 10.1016/j.apsusc.2011.01.113
[13] Ding R G, Ojo O A, Chaturvedi M C. Laser beam weld-metal microstructure in a yttrium modified directionally solidified Ni3Al-base alloy. Intermetallics, 2007, 15: 1504–1510. DOI: 10.1016/j.intermet.2007.05.008
[14] Lu J T, Zhu S L, Wang F H. Cyclic oxidation and hot corrosion behavior of Y/Cr-modified aluminide coatings prepared by a hybrid slurry/pack cementation process. Oxid Met, 2011, 76: 67–82. DOI: 10.1007/s11085-010-9228-0
[15] Monceau D, Oquab D, Estournes C, et al. Pt-modified Ni aluminides, MCrAlY-base multilayer coatings and TBC systems fabricated by Spark Plasma Sintering for the protection of Ni-base superalloys. Surf Coat Tech, 2009, 204: 771–778. DOI: 10.1016/j.surfcoat.2009.09.054
[16] Vilar R, Santos E C, Ferreira P N, et al. Structure of NiCrAlY coatings deposited on single-crystal alloy turbine blade material by laser cladding. Acta Mater, 2009, 57: 5292–5302. DOI: 10.1016/j.actamat.2009.06.049
[17] Wang K L, Zhang Q B, Sun M L, et al. Rare earth elements modification of laser-clad nickel-based alloy coatings. Appl Surf Sci, 2001, 174: 191–200. DOI: 10.1016/s0169-4332(01)00017-4
[18] Moulin P, Huntz A M, Lacombe P. Relation between selective oxidation and diffusional phenomena in Fe-Ni-Cr ternary alloys-effect of yttrium additions. Acta Metall Mater, 1980, 28: 1295–1300. DOI: 10.1016/0001-6160(80)90085-1
[19] Zhang Y D, Zhang C, Lan H, et al. Improvement of the oxidation resistance of Tribaloy T-800 alloy by the additions of yttrium and aluminium. Corros Sci, 2011, 53: 1035–1043. DOI: 10.1016/j.corsci.2010.11.038
[20] Khanna A S, Wasserfuhr C, Quadakkers W J, et al. Addition of yttrium, cerium and hafnium to combat the deleterious effect of sulfur impurity during oxidation of an Ni-Cr-Al alloy. Mat Sci Eng A-Struct, 1989, 120-121: 185–191. DOI: 10.1016/0921-5093(89)90738-7
[21] Mendis B G, Livi K J T, Hemker K J. Observations of reactive element gettering of sulfur in thermally grown oxide pegs. Scripta Mater, 2006, 55: 589–592. DOI: 10.1016/j.scriptamat.2006.06.017
[22] Schumann E, Yang J C, Graham M J. Direct observation of the interaction

of yttrium and sulfur in oxidized NiA. Scripta Mater, 1996, 34: 1365–1370. DOI: 10.1016/1359-6462(95)00662-1
[23] Xiao C B and Han Y F. Effect of silicon on microstructure and stress rupture properties at 1100 °C of yttrium modified Ni-Al-Mo-B alloy IC6. J Mater Sci, 2001, 36: 1027–1030. DOI: 10.1023/a:1004848528582
[24] Stringer J. Stress generation and relief in growing oxide films. Corros Sci, 1970, 10: 513–543. DOI: 10.1016/S0010-938X(70)80036-1

Figures

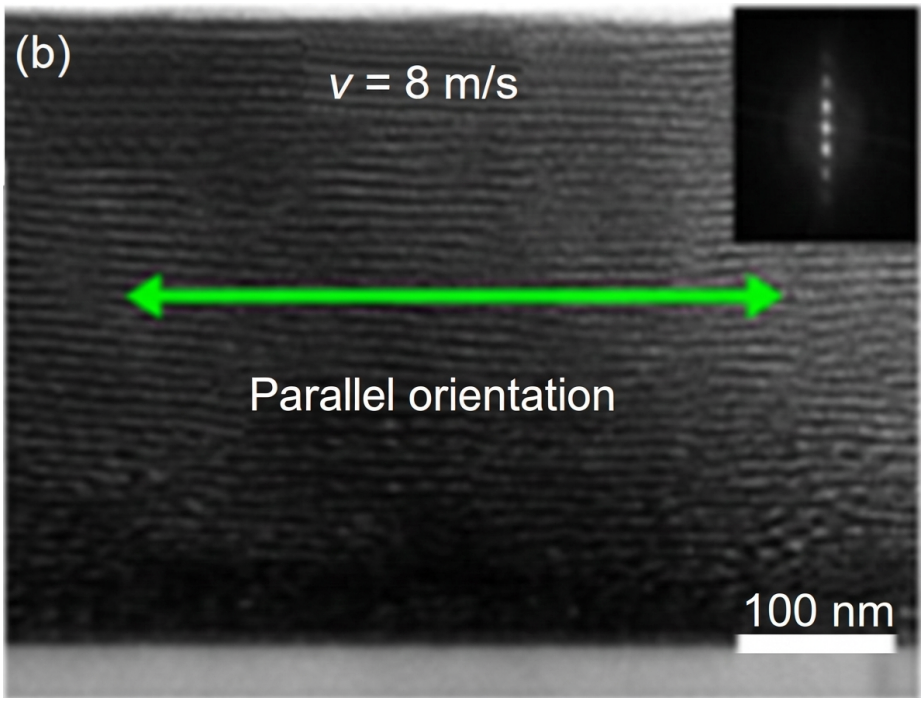

Figure 1: Figure 13

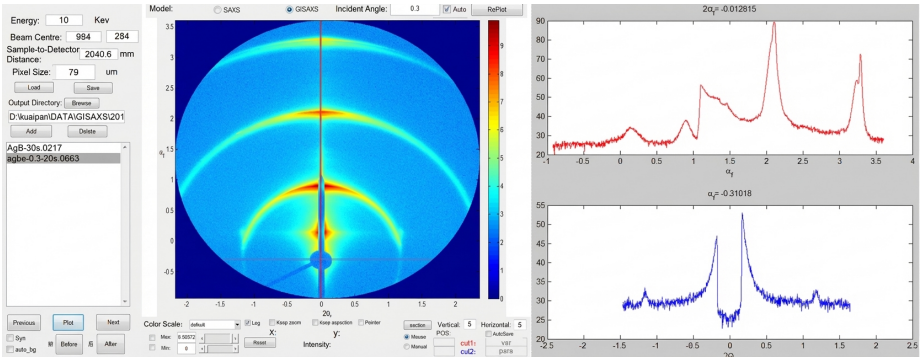

Figure 2: Figure 17